J. Fluid Mech. (2002), *vol.* 463, *pp.* 293–312.
DOI: 10.1017/S0022112002008832 Printed in the United Kingdom

Buoyancy-driven ventilation between two chambers

By Y. J. P. LIN AND P. F. LINDEN

Department of Mechanical and Aerospace Engineering, University of California, San Diego, 9500 Gilman Drive La Jolla, CA 92093-0411, USA

(Received 6 November 2001 and in revised form 25 January 2002)

A model of single-room displacement ventilation is extended to a space consisting of two chambers of equal height connected by two openings. Individually, both chambers have displacement ventilation in this geometrical arrangement, but the space itself is not connected to the outside. Thus we are considering ventilation of two chambers in the interior of a building, such as an office connected to an internal atrium. Theoretical analysis and experimental results are presented in this paper. The experiments use salt solutions to simulate thermal forcing in buildings and the theoretical analysis is based on plume theory. The two chambers have a time-dependent interaction resulting from changing stratification in the two chambers. We concentrate here on a small chamber with an internal heat source connected to a large unheated chamber, and show that the time variation is determined by the size of the larger chamber. We discuss the implications of these results for building ventilation design and control.

1. Introduction

Natural ventilation is an important issue for the building industry. Air-conditioned buildings use a large amount of energy, and natural ventilation provides an attractive alternative if it can deliver a controlled and high-quality indoor environment. In addition to energy saving, natural ventilation reduces noise from mechanical devices, avoids maintenance of mechanical equipment and assists environmental conservation by reducing emissions.

Most previous work on natural ventilation has been restricted to a single space. Linden, Lane-Serff & Smeed (1990, hereafter referred to as LLSS) developed a mathematical model of the steady-state natural displacement ventilation in a single room produced by a single steady heat source. The room is connected to an infinite homogenous environment via top openings at the ceiling and bottom openings at the floor (figure 1). After the heat source has added buoyant fluid for some time, a steady-state interface between two layers of uniform but different densities forms in the room. The height of the interface depends on the size of the openings and the height of the room but is independent of the strength of the heat source.

LLSS used the neutral pressure level concept (see § 2), volume and momentum conservation to develop a mathematical model in which the heat source is treated as a turbulent plume. The model predicts the interface height and the reduced gravity of the upper buoyant layer in the steady state. This model has been verified against experimental results in LLSS and following papers (Hunt & Linden 1999, 2001).

Cooper & Linden (1996) extended this model to two buoyancy sources with different strengths in an enclosure, and Linden & Cooper (1996) considered the problem of

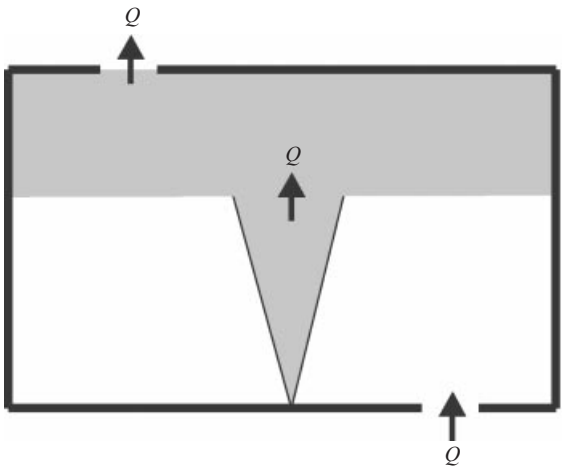

FIGURE 1. Displacement ventilation in a single room with a single heat source. In the steady state the interface height is determined only by the size of the openings and the height of the room. The upper layer temperature is uniform and equal to the plume temperature at the interface. The flow rate Q through the room is given by the volume flux in the plume at the interface height.

multiple sources in an enclosure. Hunt & Linden (1999, 2001) have examined the effects of wind on these flows.

However, buildings rarely are simple single interior spaces. They are usually subdivided into interior spaces, such as rooms and corridors. The question then arises as to how the interior geometry affects the ventilation flow. As a first step, we study two connected spaces within a building. We restrict attention here to the case where the building itself is not connected to the exterior environment. Thus we are considering two rooms within the interior of a building, neither of which has any openings to the outside. We further restrict attention to the flow generated by a steady heat source in the smaller chamber. While this is a special case, we find an interesting behaviour that justifies study and explanation. The two spaces are connected via the top and bottom openings on a shared vertical wall. Figure 2 depicts the geometrical configuration. This arrangement of openings induces displacement ventilation in both spaces.

A single heat source in an enclosed undivided space was studied by Baines & Turner (1969). They showed that outside the plume a stable stratification developed, which had a self-similar form at large times such that all the fluid within the space was heated at the same rate. This form of stratification has become known as a 'filling-box' stratification. Different arrangements of openings can cause qualitatively different flow patterns as shown by Wong & Griffiths (2001) who also studied the flows produced by plumes in two connected regions. They considered a similar situation to that studied here of a buoyant plume in one chamber but with only one opening at the bottom (see figure 3*a*). When the plume is activated the buoyant fluid fills the forced chamber (the chamber with the plume) until it reaches the height of opening and flows into the unforced chamber (the chamber without a plume). The buoyant fluid enters the unforced chamber and rises as a turbulent plume (effectively either a point or line plume depending on the geometry of the opening). The unforced chamber then develops a 'filling-box' stratification which descends until it reaches the height of the opening. After this the stratification descends in both chambers with continual flow of buoyant fluid through the opening into the unforced chamber. If there is only one opening on the top (see figure 3*b*), the unforced chamber provides

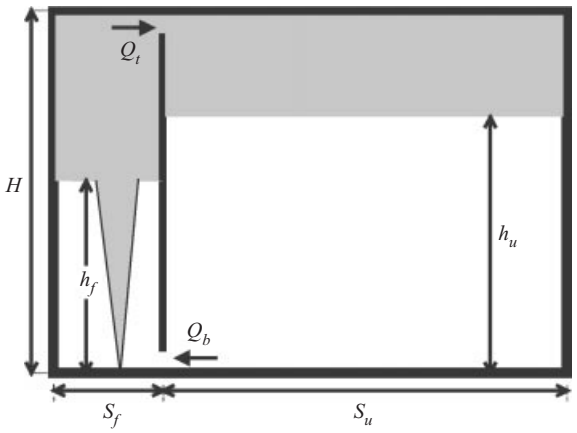

FIGURE 2. Thermal ventilation in two rooms, which are connected to each other by two openings. The top and bottom openings have areas a_t and a_b, respectively. The forced chamber of area S_f on the left has one heat source; the right chamber of area S_u is unforced.

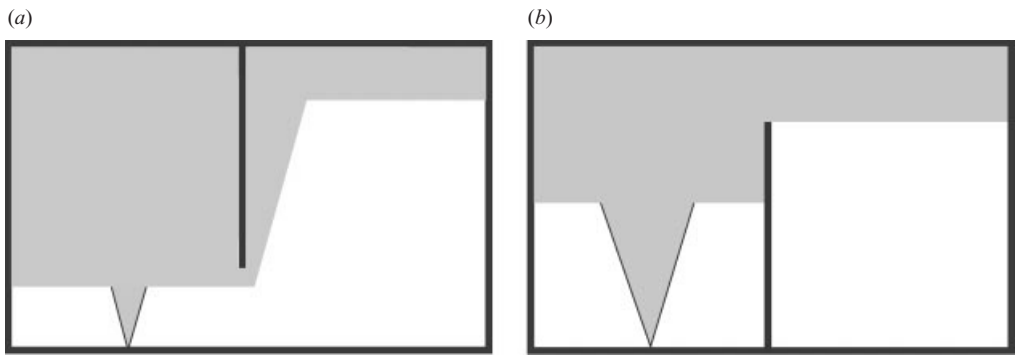

FIGURE 3. Different positions of connecting openings result in different flow patterns. (*a*) When the opening is at the bottom, the buoyant fluid fills the forced chamber until it reaches the opening and flows into the unforced chamber. (*b*) When the opening is at the top, the buoyant fluid enters the unforced chamber and stays near the ceiling, eventually isolating the fluid below the opening.

additional space to hold the buoyant fluid from the forced chamber. The buoyant fluid flows through the top opening and occupies the upper part of the unforced chamber. When the stratification descends to the bottom of the opening, cool air remains trapped in the unforced chamber, and it plays no part in the flow. This is similar to the filling box of Baines & Turner (1969); however the cross-section area is not uniform at all heights unlike the prototype model in their paper.

In our study we concentrate on a single geometry, where there are two openings of fixed size, one at the top and one at the bottom of the shared vertical wall, and examine the effects of changing the relatives sizes of the chambers. When the unforced chamber is very large compared to the forced chamber, the system acts like a heated room connected to the outside – in the limit of the unforced chamber becoming infinite this is exactly what happens and the steady state described by LLSS applies. At the other extreme, there is no unforced chamber adjacent to the forced chamber and we return to the classical filling box described by Baines & Turner (1969). When the unforced chamber is finite the flow is always unsteady, and we are concerned with the time variation of the flow and its dependence on the relative sizes of the

two chambers. In § 2 we develop a mathematical model for two connected rooms. In § 3 the experiments and the data processing are described. In § 4 the comparisons of the theoretical model and experimental results are presented. The conclusions and discussion of applications to buildings are given in § 5.

2. Theory

We extend the mathematical model of the single room in the infinite homogeneous environment presented in LLSS to the case of two coupled spaces. The two spaces are connected via the top opening and bottom opening on the shared vertical wall (figure 2). We develop a mathematical model for a heat plume source in two chambers, because thermal comfort problems in buildings are usually concerned with heat sources. However the results apply equally to a cold source located at the ceiling of the forced chamber, provided temperature differences are sufficiently small for the Boussinesq approximation to be valid. Given that typical temperature differences arising from heating or cooling in buildings are a few degrees Kelvin, this is usually the case. In the experiments described in § 3 we use a dense source on the ceiling, but we will describe the model for a hot source on the floor. For the small density differences encountered in buildings, the Boussinesq approximation can apply and this inversion gives equivalent flows.

LLSS showed theoretically that, in a single room containing one constant source of buoyancy and connected by openings at the top and bottom to an infinite homogeneous environment, the steady-state stratification consists of two layers each of uniform density. This two-layer stratification was observed in their experiments. There is a steep density gradient at the interface and the density in the hot layer is almost uniform. In this steady state the volume flux in the plume at the interface is equal to the flux through the two openings, since air can only cross the stable interface inside the buoyant plume (figure 1).

In the enclosed double-chamber case, when the width of the unforced chamber is infinite, the flow in the forced chamber is the same as that in the single room connected to an infinite environment. Therefore, when the unforced chamber is finite we assume that the stratification in the forced chamber consists of two layers with uniform but different densities. We expect this approximation to be valid when the ratio $R_A = S_u/S_f$ of their cross-sectional areas is large. Here S_u and S_f are the cross-sectional areas of the unforced and forced chambers, respectively. We will develop the model based on this assumption and check its validity in our experiments.

When the plume starts to inject buoyant fluid, it first collects at the top of the forced chamber and then flows into the unforced chamber through the top opening, and there is a corresponding inflow from the unforced chamber to the forced chamber through the bottom opening. There is a possibility that a two-way exchange flow may occur through the upper opening, particularly if it is much larger than the lower opening. In the present experiments when both openings were the same size, only unidirectional flow as described was observed. Thus both chambers have displacement ventilation: the forced chamber in the traditional sense of warm air leaving at the top displaced by cool air from beneath. On the other hand, in the unforced chamber warm air enters at the top and cool air leaves at the bottom. So while the characteristic stable stratification associated with displacement is maintained, the direction of the ventilation in the unforced chamber is downwards rather than upwards. In the unforced chamber the displacement ventilation is not driven by the buoyancy within that chamber – rather it is forced by the heated chamber.

2.1. *The ventilation model*

Since an ideal plume source does not introduce volume flux, the volume flow rates Q_t at the top opening and Q_b at the bottom opening must be equal to satisfy the volume conservation law, i.e.

$$Q_t = Q_b = Q. \tag{2.1}$$

Applying the two-layer stratification assumption in the forced chamber, the two densities there are taken to be ρ_f (the density of the buoyant layer) and ρ_w (the density of the lower layer which is also the initial density throughout the unforced chamber). The two layers are separated by a horizontal interface. Since fluid only crosses the stable density interface in the plume, if the interface remains stationary, the top and bottom fluxes are equal to the volume flux Q_p in the plume at the interface. Because the upper layer has a uniform density, the density of the buoyant layer in the forced chamber is the same as that of the plume at the interface.

As fluid flows from the upper layer of the forced chamber it forms a buoyant layer along the ceiling of the unforced chamber. Consequently, the pressure difference across the upper opening decreases. This means that Q_t decreases with time, and a smaller plume flow rate is needed. Since Q_p increases with height due to entrainment, this reduction is achieved by decreasing the interface height. The density of the fluid entering the buoyant layer in the plume then decreases and the density of that layer decreases with time. Fluid entering the unforced chamber fluid becomes less dense with increasing time and so flows along the ceiling on top of fluid that entered earlier. This process produces a stable stratification in the unforced chamber, which we represent by $\rho_u(z)$.

Although the build up of stable stratification is similar to that in the classical filling box, the process itself is quite different. In the filling box, the stratification is produced by re-entrainment of buoyant fluid by the plume. Here it is associated with a lowering of the interface in the forced chamber caused by the presence of buoyant fluid in the unforced chamber.

The pressure distributions in the two chambers are represented in figure 4, where P_f and P_u denote the pressures in the forced and unforced chambers, respectively. The neutral level is the height where pressures in the two chambers are equal and is denoted by h_n in figure 4.

Noting that the neutral level is always above the level of the interface in the forced chamber, we construct the formulae for the exchange flow rates and interface heights as follows. The pressures at the top of the two rooms are

$$P_f(H) = P_n - g\rho_f(H - h_n) \tag{2.2a}$$

and

$$P_u(H) = P_n - g\rho_w(h_u - h_n) - g\int_{h_u}^{H} \rho_u(z)\,\mathrm{d}z, \tag{2.2b}$$

where h_f and h_u are interface heights in the forced and unforced chambers, respectively, as depicted in figures 2 and 4, and P_n is the pressure at the neutral level. The pressures at the bottom of the two rooms are

$$P_f(0) = P_n + g\rho_f(h_n - h_f) + g\rho_w h_f \tag{2.3a}$$

and

$$P_u(0) = P_n + g\rho_w h_n. \tag{2.3b}$$

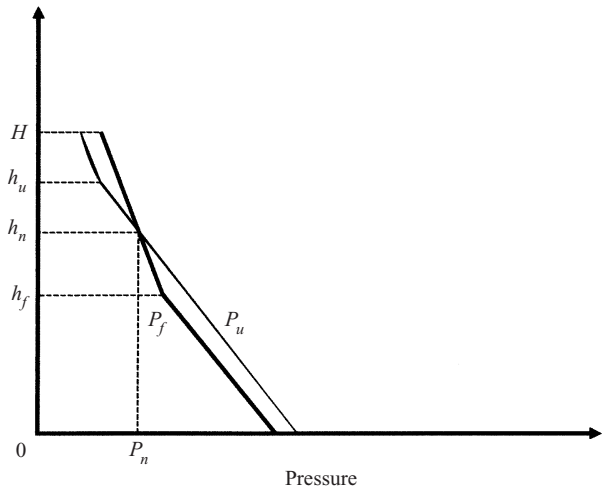

FIGURE 4. The thicker solid line represents the pressure profile P_f in the forced chamber and the thinner line represents the pressure profile P_u in the unforced chamber. The neutral level where the pressures are equal in the two connected rooms is h_n. The plume source is at $z = 0$. This pressure diagram corresponds to figure 2.

The pressure differences across the openings at the top and the bottom are

$$\Delta P_t = P_f(H) - P_u(H) = g\rho_w(h_u - h_n) + g\int_{h_u}^{H} \rho_u(z)\,\mathrm{d}z - g\rho_f(H - h_n) \tag{2.4a}$$

and

$$\Delta P_b = P_u(0) - P_f(0) = g(\rho_w - \rho_f)(h_n - h_f). \tag{2.4b}$$

The pressure differences ΔP_t, ΔP_b are positive, since $P_f(H) > P_u(H)$ and $P_u(0) > P_f(0)$ (see figure 4).

The density difference $\Delta\rho_f = \rho_w - \rho_f$ between the homogeneous buoyancy layer ρ_f and fresh ambient layer ρ_w is small compared to ρ_w, so that the Boussinesq approximation is valid. Let $g'_f = g(\rho_w - \rho_f)/\rho_w$ and $g'_u(z) = g(\rho_w - \rho_u(z))/\rho_w$ represent the reduced gravities in the forced chamber and unforced chamber, respectively. The buoyancy conservation equation for the total space is

$$Bt = S_f g'_f(H - h_f) + S_u \int_{h_u}^{H} g'_u(z)\,\mathrm{d}z, \tag{2.5}$$

where B is the buoyancy flux in the plume and t is the time measured from when the plume is turned on.

We write the flows through the top and bottom openings caused by pressure differences as

$$\rho_f Q_t^2 = A_t^{*2}\Delta P_t \tag{2.6a}$$

and

$$\rho_w Q_b^2 = A_b^{*2}\Delta P_b, \tag{2.6b}$$

respectively. Here $A_t^* = \sqrt{2}c_t a_t$ and $A_b^* = \sqrt{2}c_b a_b$ are the effective areas of the top and bottom openings. The coefficients c_t and c_b represent the effects of turbulent losses and contractions at the openings. To be consistent with previous work (see Cooper & Linden 1996) we take $c_t = 0.6$ and $c_b = 0.7$.

Summing equations (2.6*a*) and (2.6*b*) and substituting ΔP_t and ΔP_b from (2.4*a*) and (2.4*b*), we find

$$\begin{aligned}\rho_f \frac{Q_t^2}{A_t^{*2}} + \rho_w \frac{Q_b^2}{A_b^{*2}} &= g\left(\rho_f(h_f - H) + \rho_w(h_u - h_f) + \int_{h_u}^{H} \rho_u(z)\,\mathrm{d}z\right),\\ &= g\rho_w\left(\frac{\rho_w - \rho_f}{\rho_w}\right)(H - h_f) - g\rho_w \int_{h_u}^{H} \frac{\rho_w - \rho_u(z)}{\rho_w}\,\mathrm{d}z,\\ &= \rho_w\left(g_f'(H - h_f) - \int_{h_u}^{H} g_u'(z)\,\mathrm{d}z\right). \end{aligned} \tag{2.7}$$

Using the Boussinesq approximation ($\rho_f \approx \rho_w$), (2.7) becomes

$$\frac{Q_t^2}{A_t^{*2}} + \frac{Q_b^2}{A_b^{*2}} = g_f'(H - h_f) - \int_{h_u}^{H} g_u'(z)\,\mathrm{d}z. \tag{2.8}$$

Define, as in LLSS the effective area A^* of the openings,

$$A^* = \frac{a_t a_b}{(\frac{1}{2}(a_b^2/C_t^2 + a_t^2/C_b^2))^{1/2}}, \tag{2.9a}$$

which can be expressed in terms of A_t^* and A_b^* as

$$\frac{1}{A^{*2}} = \left(\frac{1}{A_t^{*2}} + \frac{1}{A_b^{*2}}\right). \tag{2.9b}$$

Using the effective area A^* by (2.9*b*) and volume conservation equation (2.1), (2.8) becomes

$$\frac{Q^2}{A^{*2}} = g_f'(H - h_f) - \int_{h_u}^{H} g_u'(z)\,\mathrm{d}z. \tag{2.10}$$

Using buoyancy conservation (2.5), we can replace $\int_{h_u}^{H} g_u'(z)\,\mathrm{d}z$ with known parameters S_u, S_f, B, t, g_f', and then (2.10) becomes

$$\begin{aligned}\frac{Q^2}{A^{*2}} &= g_f'(H - h_f) - \frac{1}{S_u}(Bt - S_f g_f'(H - h_f)),\\ &= g_f'(H - h_f)\left(1 + \frac{1}{R_A}\right) - \frac{Bt}{S_u}, \end{aligned} \tag{2.11}$$

where we recall that $R_A = S_u/S_f$.

2.2. *The forced chamber*

In the forced chamber, the volume flux in the plume at the interface is equal to the sum of the outflow volume flux into the unforced chamber and the rate of increase in the volume of the upper layer, i.e.

$$Q_p(h_f, B) = Q_t + S_f w_f(t) = Q + S_f w_f(t), \tag{2.12}$$

by (2.1), where $w_f = \mathrm{d}h_f/\mathrm{d}t$ is the velocity of the changing interface in the forced chamber.

Substituting equation (2.12) into (2.11), we obtain equations for the time evolution of the exchange flow rate and the interface height in the forced chamber:

$$Q_p(h_f, B) - S_f w_f(t) = A^*\left(g_f'(H - h_f)\left(1 + \frac{1}{R_A}\right) - \frac{Bt}{S_u}\right)^{1/2} \tag{2.13}$$

and

$$w_f(t) = \frac{1}{S_f}\left(Q_p(h_f, B) - A^*\left(g'_f(H-h_f)\left(1+\frac{1}{R_A}\right) - \frac{Bt}{S_u}\right)^{1/2}\right). \tag{2.14}$$

Morton, Taylor & Turner (1956), using the entrainment assumption, derived the equations of the reduced gravity g'_p and volume flux Q_p in a plume, in terms of the buoyancy flux B and distance z from the source. In the initially homogeneous environment

$$B = g'_p Q_p = \text{constant}, \tag{2.15a}$$

$$g'_p = g'_p(z, B) = (B^2 z^{-5})^{1/3}/C \tag{2.15b}$$

and

$$Q_p = Q_p(z, B) = C(Bz^5)^{1/3}, \tag{2.15c}$$

where z is measured from the source origin. In equation (2.15), the universal constant $C = 6\alpha/5(9\alpha/10)^{1/3}\pi^{2/3}$, where α is the entrainment constant, which is the ratio of the entrainment velocity into the plume to the mean vertical velocity at any height.

Substitution of the plume equations (2.15b) and (2.15c) in the interface evolution equation (2.14) gives

$$\frac{\mathrm{d}h_f}{\mathrm{d}t} = \frac{1}{S_f}\left(C(Bh_f^5)^{1/3} - A^*\left(\frac{(B^2h_f^{-5})^{1/3}}{C}(H-h_f)\left(1+\frac{1}{R_A}\right) - \frac{Bt}{S_u}\right)^{1/2}\right). \tag{2.16}$$

There are two extreme cases to verify this equation. One is the Baines & Turner (1969) filling box when the $S_u = 0$, and the other is from LLSS when there is an infinite homogeneous environment $S_u = \infty$ outside the forced chamber.

When $S_u = 0$, (2.5) implies $Bt = S_f g'_f(H - h_f)$, and the buoyant fluid is all included in one fixed space. For this filling-box case (2.16) becomes

$$\frac{\mathrm{d}h_f}{\mathrm{d}t} = \frac{1}{S_f}C(Bh_f^5)^{1/3} = \frac{1}{S_f}Q_p(h_f, B). \tag{2.17}$$

The interface growth rate given by (2.17) is determined by the plume flow rate at the interface $Q_p(h_f, B)$ and cross-section area S_f. This relation is equivalent to the equation for the growth of the stratified layer in the filling box in Baines & Turner (1969) (see their equation (3)). In their paper, the cross-section area is πR^2 and the volume flux is $\pi b^2 w$, where b is the radius and w is the vertical velocity at the interface of plume. However, our model only predicts the descent of the stratification region in this limit but not the stratification since we assume a two-layer stratification. The correct descent rate is obtained since it only depends on entrainment into the plume below the stratified region.

When $S_u = \infty$, the terms $1/R_A$ and Bt/S_u in (2.16) are zero. So when the interface height is at the value given in LLSS

$$\frac{\mathrm{d}h_f}{\mathrm{d}t} = 0,$$

and the interface is steady. Therefore (2.16) is reduced to

$$C(Bh_f^5)^{1/3} = A^*\left(\frac{(B^2h_f^{-5})^{1/3}}{C}(H-h_f)\right)^{1/2}. \tag{2.18}$$

The left-hand-side term of (2.18) is the volume flux in the plume at the interface, and right-hand-side term is the exchange flow rate Q with the outside environment. This is the same result as obtained by LLSS: the volume flux in the plume at the interface is equal to the exchange flow rate at the top and bottom openings.

We can make (2.18) non-dimensional with the height H of the chamber to obtain

$$\frac{A^*}{H^2} = C^{3/2}\left(\frac{\xi_f^5}{1-\xi_f}\right)^{1/2}, \tag{2.19}$$

where $\xi_f = h_f/H$ is the non-dimensional height of the interface in the forced chamber, and (2.19) is the same as (2.11*a*) in LLSS.

We use the chamber depth H and the time scale T to make (2.16) non-dimensional. We choose T to be the time scale proportional to the filling-box time for the unforced chamber,

$$T = \frac{S_u H}{B^{1/3}H^{5/3}} = \frac{S_u}{B^{1/3}H^{2/3}}. \tag{2.20}$$

The numerator of (2.20) is the volume of the unforced chamber and the denominator is proportional to the volume flux in the plume at the top of the forced chamber and so T is proportional to the time taken for all the fluid in the unforced chamber to be circulated through the plume. Let τ represent the non-dimensional time $\tau = t/T = B^{1/3}H^{2/3}t/S_u$.

Multiply (2.16) by T/H to obtain the non-dimensional interface evolution equation

$$\frac{\mathrm{d}\xi_f}{\mathrm{d}\tau} = R_A\left(C\xi_f^{5/3} - \frac{A^*}{H^2}\left(\frac{1}{C}\xi_f^{-5/3}(1-\xi_f)\left(1+\frac{1}{R_A}\right) - \tau\right)^{1/2}\right). \tag{2.21}$$

The evolution of the interface in a filling box depends only on the cross-section area and the volume flux across the density interface from (2.17). When a single room connects to an infinite environment, (2.19) shows that the effective area A^* and height H determine the density interface position. Here, a room with a heat source is adjacent to an unforced room of finite volume, and the interface evolution becomes more complicated than before. Two additional parameters are introduced in (2.21). These two new parameters are T, which is the time scale to fill the unforced chamber with fluid from the plume and determines the dimensionless time τ, and R_A, which is the ratio of the cross-section areas of the two rooms.

2.3. *The unforced chamber*

The unforced chamber receives buoyant fluid through the top opening. The interface evolution rate in the unforced chamber depends on the cross-section area of unforced chamber S_u and exchange flow rate Q_t, i.e.

$$Q_t = w_u(t)S_u = \frac{\mathrm{d}h_u}{\mathrm{d}t}S_u. \tag{2.22}$$

Combining (2.13) and (2.22) we obtain

$$\frac{\mathrm{d}h_u}{\mathrm{d}t} = \frac{A^*}{S_u}\left(g_f'(H-h_f)\left(1+\frac{1}{R_A}\right) - \frac{Bt}{S_u}\right)^{1/2}. \tag{2.23}$$

Substituting g_f' by (2.15*b*) in (2.23), then using the time scale T defined by (2.20)

and the length scale H to make (2.23) non-dimensional gives

$$\frac{\mathrm{d}\xi_u}{\mathrm{d}\tau} = \frac{A^*}{H^2}\left(\frac{1}{C}\xi_f^{-5/3}(1-\xi_f)\left(1+\frac{1}{R_A}\right)-\tau\right)^{1/2}, \tag{2.24}$$

where $\xi_u = h_u/H$ is the non-dimensional upper layer depth in the unforced chamber.

The reduced gravity of the fluid entering the unforced chamber is the same as that in the forced chamber, i.e.

$$g'_u(1,\tau) = g'_f(\tau). \tag{2.25}$$

The buoyant fluid is assumed to spread out horizontally instantaneously as a homogeneous thin layer. The fluid entering at later times flows on top of the fluid that previously entered. This is an idealized assumption. In reality, the reduced gravity change in this room is due to the propagation of a gravity current, which has a finite depth and takes a finite time to propagate across the unforced chamber. This is not an ideal model for a short time period; however it is close to the experiment when the time period is long.

In numerical calculations, we solve $g'_f(\tau)$ and $\xi_u(\tau)$ simultaneously and in every time interval $\Delta\tau$ we assume that the new thin layer entering (the dimensionless thickness is $\Delta\xi_u(\tau_1) = |\xi_u(\tau_1+\Delta\tau) - \xi_u(\tau_1)|$) has the homogeneous reduced gravity ($g'_f(\tau_1)$), the reduced gravity in the forced chamber at that moment. The previous fluid layers are all moved downwards a distance $\Delta\xi_u$. Then the numerical calculations of the reduced gravity in the unforced chamber at different moments $g'_u(\xi,\tau)$ are obtained as a simple initial value problem. We will present the numerical calculations together with the experimental results in § 4.

3. Experiments

The experiments were conducted in a Plexiglas tank 122 cm long, 15.6 cm wide and 59 cm deep. Two dividers, one 15.6 cm wide by 46 cm high and the other 15.6 cm wide by 59 cm high, and both 2 cm in thickness, were used to subdivide the tank. The smaller divider (15.6 cm by 46 cm) was placed inside the tank to form a fixed 15 cm wide space which was the forced chamber, connected to the other space via the top and bottom openings. When the tank is filled with fresh water to 49 cm high, the openings at the top and bottom are both 1.5 cm in height. The larger divider was placed at different positions in the other side of tank to form the unforced chamber. Its length varied from 15 cm to 105 cm at 30 cm intervals, giving ratios R_A of the two chambers from 1 to 7. Refer to figure 5 for a sketch of the experimental design.

Fresh water was used as the ambient fluid and replenished in each experiment. A plume nozzle was placed in the centre of forced chamber and supplied by a constant-head source of salt solution with density $\rho_s = 1.117\,\mathrm{g\,cm^{-3}}$. The orientation in this section and in § 4 is upside down compared with the coordinate system of theoretical thermal model in § 2 (see figure 2). However, the coordinate system is consistent throughout the paper, and the plume nozzle is always positioned at $z = 0$. The description of the experimental results will be in terms of the orientation of the experiments. Blue food dye was added to the salt solution to make injected fluid visible. A flow meter regulated a constant flux of buoyant fluid into the tank. The plume nozzle was designed by Dr Paul Cooper in the Department of Engineering, University of Wollongong, NSW, Australia, and details can be found in Hunt & Linden (2001).

A shield of transparent Plexiglas sheet (12 cm high by 12 cm wide) was placed near

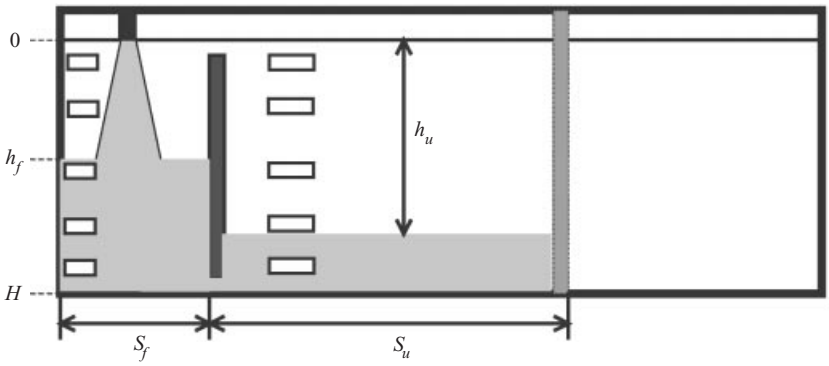

FIGURE 5. The experimental arrangement shows the forced chamber on the left and the unforced chamber on the right. A plume nozzle, located at the free surface, is placed at the centre of the left chamber. The columns of windows for measuring light intensity in both chambers are also depicted.

the top of the forced chamber between the plume nozzle and the smaller divider to reduce plume deflection due to the flow through the top opening into the forced chamber.

Experimental data were recorded on digital files and videotape. Videotape recording requires signals to pass through the VCR (Video Cassette Recorder) and then be recorded onto tape. Both procedures add nonlinear effects to the signals, which makes later analysis complicated. Therefore, we only used videotape recordings as reference data. DigImage, an image processing software developed by Dalziel (1993), was used to record and analyse the experimental data. Images were recorded through a Cohu 7710 series CCD camera directly into the computer hard drive. The linear gain of the CCD camera and direct recording onto digital files reduce noise and simplify later analysis.

The light attenuation due to the dye in the salt solution is related to the density of the solution, since the dye is added in proportion to the salt concentration. The details of this technique are given by Cenedese & Dalziel (1998), and the basics are as follows. Before running experiments, we used the same lighting as in the experiments to record images of sample solutions and measured their densities with an Anton Paar densitometer. We used the light intensities of the samples and their measured densities to interpolate the density distribution in the tank from images taken in experiments.

The experiment started when the plume was turned on. The flow meter maintained a constant flow $Q_f = 2.1\,\mathrm{ml\,s^{-1}}$ of brine through the plume nozzle into the tank during the entire experiment. This flow rate was small compared to the exchange flow between the two chambers, which was the volume flux in the plume at the interface, so that the source volume flux was negligible in the experiments. DigImage took an image every 20 s and the VCR recorded the whole experiment while it was running. The experiment was stopped when the front of dense fluid in the unforced chamber reached the top opening and began to flow back into the forced chamber.

Images taken in the experiment were used to analyse the evolution of density in both chambers. The average light intensity of a small window, which was 2 pixels high by 14 pixels wide (about 0.3 cm high by 2.0 cm wide in real scale) in the forced chamber and 2 pixels high by 45 pixels wide (0.3 cm high by 6.8 cm wide) in the unforced chamber, was evaluated by DigImage. Every image had two columns of windows. The column of windows in the forced chamber was positioned outside

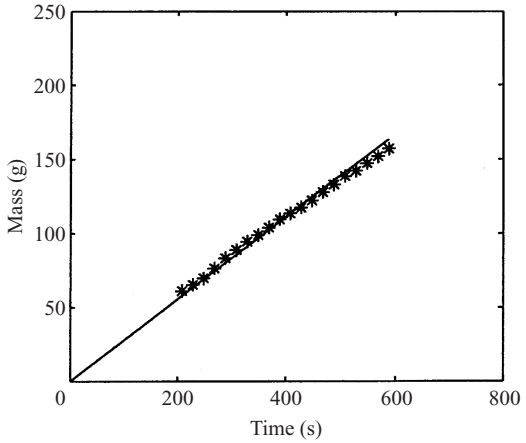

FIGURE 6. The comparison of the mass added through the plume source and the mass calculated in the tank for $R_A = 5$. The solid line is the added mass against time, using the reading from the flow meter and the supply density. The points (*) are the mass calculated from images taken during the course of the experiment. In general the two masses balance to within 10%.

the plume to monitor the evolution of the chamber environment. The centre of the window column in the unforced chamber was positioned 11.5 cm from the small divider. The column consisted of 97 windows in the forced chamber, from 0.5 cm to 48.5 cm originating from the plume nozzle with 0.5 cm vertical interval between two adjacent windows. There were 48 windows, from 1 cm to 48 cm with 1 cm vertical interval, in the unforced chamber, placed where the stratified flow developed without too much disturbance by the flow from the forced chamber and the effect of the sidewall. Figure 5 also shows a sketch of the windows in an image. The average intensity values were translated into the density values using the calibration data. In this way vertical density profiles in both chambers were obtained throughout the duration of an experiment.

The total mass added to the tank at the time when an image is taken is compared with the mass obtained from the image. Assuming the vertical density profile is independent of horizontal position in both chambers, we use the measured density profiles in each chamber to calculate the total mass in the tank from each image. Although the density profiles are not uniform everywhere in these two chambers, especially at the two ends of the unforced chambers as we mentioned before, there is an excellent agreement between total mass values calculated in these two ways as shown in figure 6.

The consistency in the mass balance was within $\pm 10\%$ for all experiments and usually considerably better. Given that the flow meter accuracy was not better than $\pm 2\%$, we consider that this level of deviation is acceptable and that the density measurement is reliable.

The light source is a fluorescent light positioned directly behind the tank and the camera is positioned 2.5 m in front of tank. The recorded image area is 59 cm by 59 cm in the tank, which is the area illuminated by the fluorescent light. Figure 7 shows a series of photos for two rooms with $R_A = 5$, after variations in background lighting have been removed.

In the experiments, the plume source has a finite volume flux and momentum flux at its origin, contrary to the pure plume theory, which assumes that the plume is a source of buoyancy only. Therefore, we need to adjust the real plume origin in the

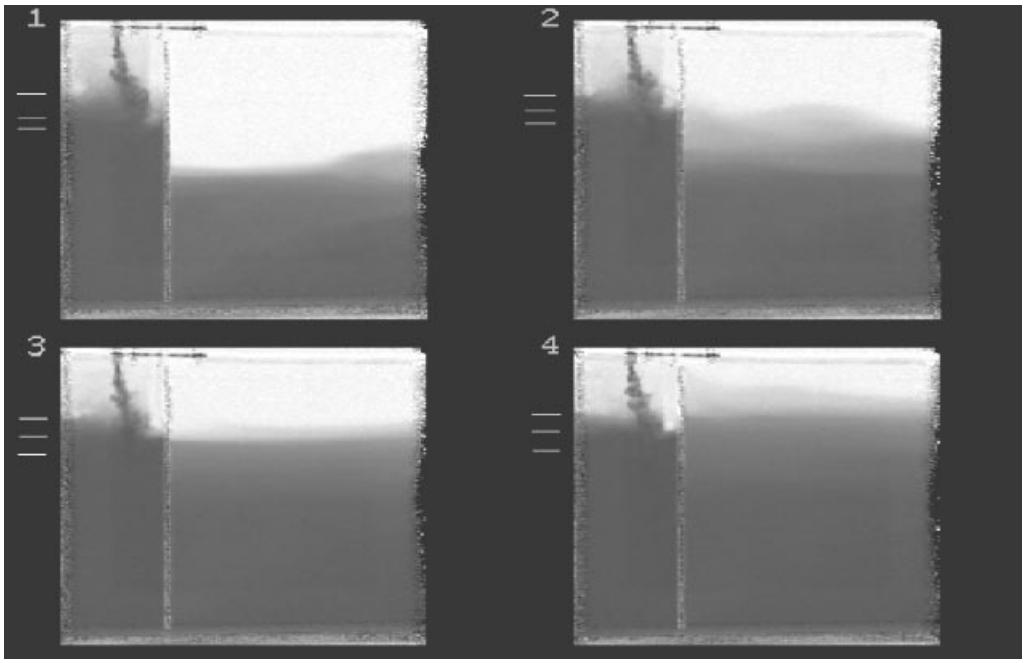

FIGURE 7. Images taken 310, 390, 470 and 550 s after the plume nozzle is turned on for the case $R_A = 5$. The corresponding non-dimensional times are $\tau = 22$, 28, 34 and 40. The horizontal white lines beside the pictures show the region of sharp density gradient that is about 12% of the total height, and the middle line in each picture is the interface height in the forced chamber, calculated as described in § 4.

experiment to fit pure plume theory and to do this we introduce the virtual origin. At the virtual origin the plume has no volume and momentum fluxes. Depending on the plume source properties, we can obtain a virtual origin height, the distance between the real and virtual plume sources. Hunt & Kaye (2001) give a detailed discussion on the virtual origin in their paper. We use equation (34) in their paper to calculate the virtual origin height z_v where $z_v > 0$ implies that the virtual origin is below the plume source. In our experiments, the buoyancy flux $B = 265\,\mathrm{cm^4\,s^{-3}}$, the reduced gravity $g' = 118\,\mathrm{cm\,s^{-2}}$, the volume flux $Q_f = 2.1\,\mathrm{cm^3\,s^{-1}}$ and the diameter of plume nozzle is 0.5 cm; therefore the virtual origin correction is $z_v = 1.66$ cm.

4. Results

When the plume is turned on dense fluid arrives at the bottom of the tank. Some of this fluid flows through the bottom opening into the unforced chamber while the rest accumulates to form a dense layer in the forced chamber. Figure 8 shows the density profiles measured in the forced and unforced chambers for the area ratio $R_A = 5$. The depth is normalized with the total depth H and the reduced gravity with $G' = (B^2(H + z_v)^{-5})^{1/3}/C$, the plume reduced gravity at the base of the tank. The profiles were measured at $\tau = 22, 28, 34$ and 40, corresponding to the images shown in figure 7. Note that the profiles begin at $g'/G' = 1$. For lower values of g'/G' the profiles are noisy due to resolution problems with the dye intensity measurements.

These images are taken at equal time intervals after the initial stage. In the initial stage the flow in the forced chamber is very disturbed and is difficult to

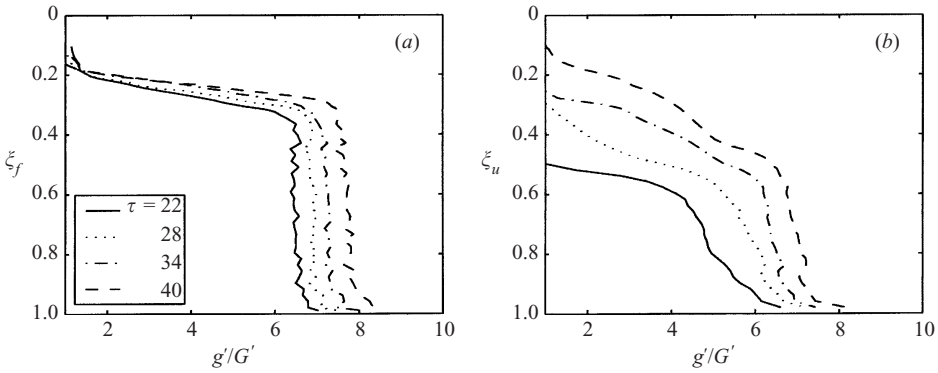

FIGURE 8. The normalized vertical reduced gravity profiles in (*a*) the forced chamber and (*b*) the unforced chamber. The four profiles were measured at $\tau = 22$, 28, 34 and 40, corresponding to the four images shown in figure 7.

analyse. Therefore, we only do some qualitative analysis for this stage without the quantitative comparisons. However, we are more concerned about the behaviour of the latter stages and both qualitative and quantitative results are presented.

The profiles in the forced chamber show an interface where there is a rapid transition of density from ambient values to a dense lower layer. This lower layer has almost uniform density with height (figure 8*a*), which supports our assumption that the two-layer stratification found for an isolated chamber with displacement ventilation is maintained here. The density and depth of this lower layer increase with time. This behaviour is consistent with the density of this layer being equal to the plume density at the interface height.

The profiles in the unforced chamber (figure 8*b*) show a more gradual vertical stratification, resulting from the displacement of the fluid vertically by new fluid entering through the bottom opening. Note that at each time the density at the bottom of the unforced chamber is equal to that in the forced chamber, consistent with the model assumption (2.25).

From the images, it is impossible to determine unambiguously the height of the interface in the forced chamber. Typical image data (figure 7) have density profiles as in figure 8(*a*), which show that the reduced gravity increases from that of the fresh water ($g' = 0$) to the average value of the lower layer (g'_f) across an interface of finite thickness, which is usually about 12% of the total height in our experiments.

In order to determine the mean interface position in the forced chamber we average the density values of those points below a non-dimensional height 0.5 (figure 8*a*), for the density ρ_f in the lower layer. The interface position is taken as the height at which $\Delta\rho_{int} = 0.6\Delta\rho_f$ (where $\Delta\rho$ is the density difference with the fresh water density $0.998\,\mathrm{g\,cm^{-3}}$). The interface position calculated in this way is shown on the images in figure 7. As can be seen from the figure the interface is not perfectly horizontal and is slightly lower at the right due to inflow through the top opening from the unforced chamber. However, the calculated position is consistent with a rough visual estimate.

The dense layer in the forced chamber initially grows rapidly in height, and then ascends more gradually. Figure 9 shows non-dimensional interface height ξ_f plotted against non-dimensional time τ in the forced chamber at four different ratios $R_A = 1, 3, 5, 7$. Results from both the experiments and the numerical calculations are shown in this figure, and the rapid initial growth and the subsequent slower rise of the interface are clearly revealed. The initial behaviour mainly depends on the size of

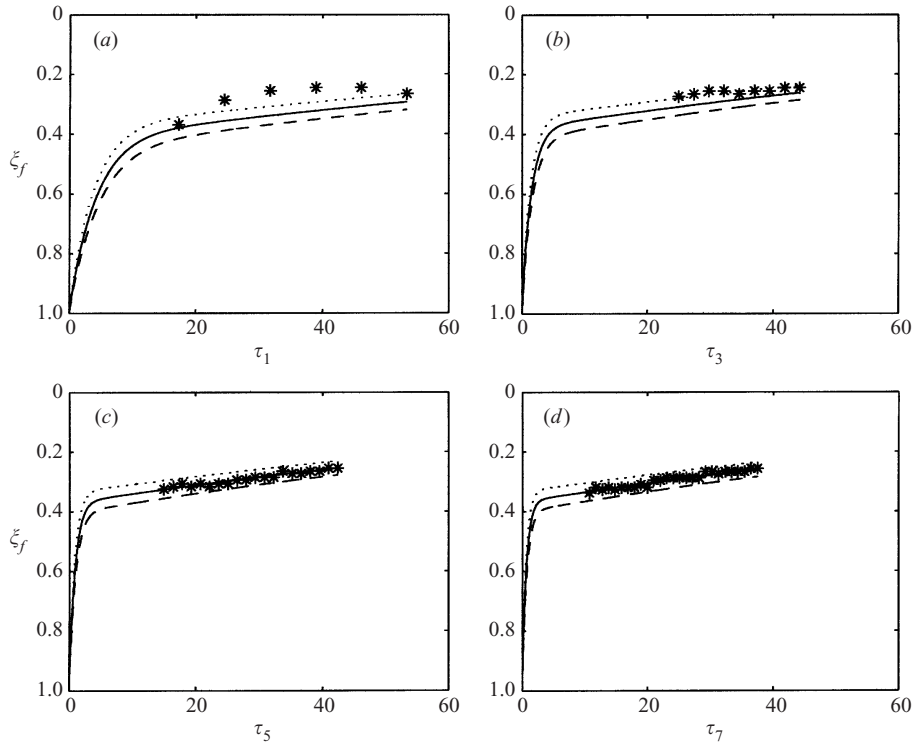

FIGURE 9. The numerical (lines) and experimental (*) interface heights in the forced chamber plotted against non-dimensional time for four different area ratios, (*a*) $R_A = 1$, (*b*) $R_A = 3$, (*c*) $R_A = 5$ and (*d*) $R_A = 7$. The three lines on each plot are numerical results with entrainment constant values $\alpha = 0.074$ (dashed line), $\alpha = 0.083$ (solid line) and $\alpha = 0.094$ (dotted line). Note that the dimensionless times are different in each plot as they are based on the horizontal area of the unforced chamber.

the forced chamber while the later stage depends on the stratification of the unforced chamber which, in turn, depends on the size of that chamber. The size of openings also has some effect on initial growth since it determines how quickly the forced chamber exchanges fluid with the unforced chamber. If the unforced chamber were infinite in extent, a steady state would be achieved with inflow and outflow of the forced chamber equal to the plume volume flux at the interface and the interface would remain stationary (LLSS). The behaviour in the initial phase is very similar to this case and the interface ascends to a value close to that for a chamber connected to an infinite environment. Using the steady-state formula (2.19), the forced chamber has the interface height $\xi_f = 0.31$ (with $\alpha = 0.083$) with these two openings, which is close to the observed values (figure 9).

We use (2.21) to calculate the height of the interface in the forced chamber as an initial value problem. As we mentioned in § 3, the real plume origin needs some modification to fit the theoretical formula. The distance parameter z in the plume equations (2.15) is replaced by $z_e = z + z_v$ and (2.21) is modified to

$$\frac{\mathrm{d}\xi_f}{\mathrm{d}\tau} = R_A S_f \left(C(\xi_f + k)^{5/3} - \frac{A^*}{H^2} \left(\frac{1}{C}(\xi_f + k)^{-5/3}(1 - \xi_f)\left(1 + \frac{1}{R_A}\right) - \tau \right)^{1/2} \right), \quad (4.1)$$

where $k = z_v/H = 0.034$.

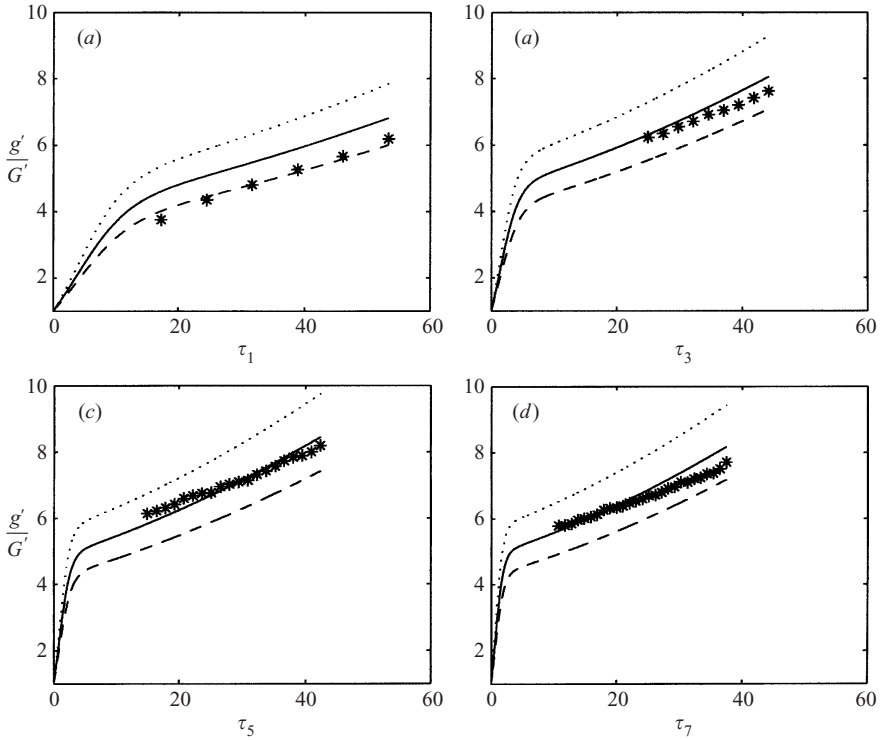

FIGURE 10. The normalized reduced gravity values in the forced chamber from the numerical calculation (lines) and the experimental measurements (*) against non-dimensional time for four area ratios. (*a*) $R_A = 1$, (*b*) $R_A = 3$, (*c*) $R_A = 5$ and (*d*) $R_A = 7$. The lines are numerical values with the three entrainment constants used in figure 9.

The numerical solutions use three different plume entrainment constants $\alpha = 0.074$, 0.083 and 0.094 to predict the interface position. These values of α are suggested by Baines (1983), Turner (1986) and Morton *et al.* (1956), respectively. The experimental data agree well with the model results and the best fit for $R_A = 5$ and 7 is achieved with $\alpha = 0.083$, consistent with other studies on ventilation (Linden 1999).

As mentioned above, the results given in figure 9 show that there are two time scales for the development of the interface in the forced chamber. The initial time scale is associated with the plume filling the smaller forced chamber and on these plots, non-dimensionalized by the size of the large unforced chamber, they do not collapse onto a single curve. Had time been made dimensionless using S_f, then the early-time growth of the interface height in each experiment would collapse onto the same curve. The subsequent increase in interface height, associated with filling the unforced chamber, scales on τ as can be seen from the figure. The agreement between the model and the data improves as R_A increases. When $R_A \approx 1$, the two time scales are quite similar and the separation of scales assumed in the model is less well satisfied.

The predicted interface height h_f is used to estimate the reduced gravity in the dense layer of the forced chamber from (2.15*b*). The height z in this equation is substituted by $h_f + z_v$ to allow for the vertical origin correction. Figure 10 shows numerical solutions and experimental data for the reduced gravity in the lower layer of the forced chamber normalized by G', the reduced gravity in the plume at the base of the tank.

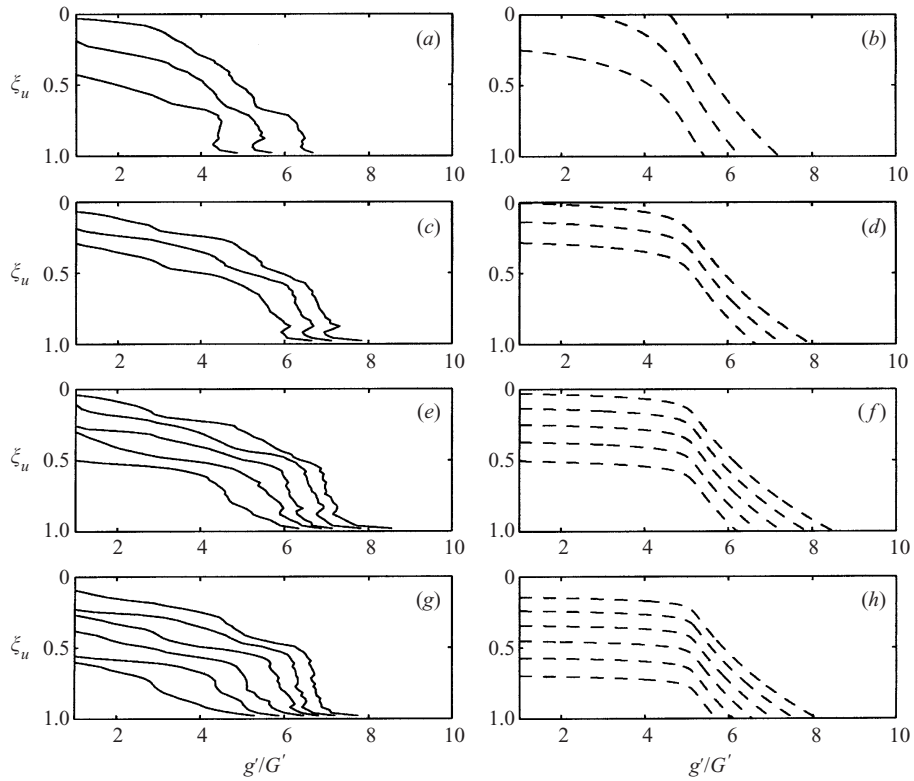

FIGURE 11. The experimental results (a, c, e, g) and numerical calculations (b, d, f, h) for the dimensionless reduced gravity in the unforced chamber. (a, b) $R_A = 1$ and non-dimensional time interval $\Delta\tau$ between two adjacent lines is $\Delta\tau = 3$. (c, d) $R_A = 3$ and $\Delta\tau = 9$. (e, f) $R_A = 5$ and $\Delta\tau = 14$. (g, h) $R_A = 7$ and $\Delta\tau = 20$.

The reduced gravity increases with time as observed in figure 8, and this increase is associated with the plume entering the layer closer to its source. As explained above, the initial values were not captured by the image analysis but the later results showed good agreement with the model calculations, with $\alpha = 0.083$ giving the closest match with the data. In this case agreement is excellent for all $R_A > 1$. When $R_A = 1$ the model slightly over-predicts the density. As with the interface height the later time development scale is on the 'filling-box' time of the unforced chamber, and when $R_A = 1$ the time scales of the two chambers are the same. Consequently, the assumption that the forced chamber forms a two-layer stratification while the unforced chamber develops over a longer time is not satisfied.

Once the reduced gravity in the lower layer in the forced chamber is known, we can calculate the interface growth in the unforced chamber as described by (2.24). Using the virtual origin again, we have the modified formula

$$\frac{\mathrm{d}\xi_u}{\mathrm{d}\tau} = \frac{A^*}{H^2}\left(\frac{1}{C}(\xi_f + k)^{-5/3}(1 - \xi_f)\left(1 + \frac{1}{R_A}\right) - \tau\right)^{1/2}. \tag{4.2}$$

The numerical solutions of non-dimensional height against non-dimensional reduced gravity at different times for four cases are presented in figure 11 to compare with the experimental measurements. Here, to avoid clutter we only use the entrain-

ment constant $\alpha = 0.083$ in the numerical calculations. This value is chosen because it gives the best fit to the experimental results in the forced chamber, and agrees with the value selected by Turner (1986) for top-hat profiles.

The reducing flow rate with time can be observed from figure 11. In these plots the spacing between two interface levels in the unforced chamber, which is the same time interval in each pair of plots, becomes smaller with time. This behaviour is more obvious at early times; there is an almost constant exchange flow at later times.

The flow entering the unforced chamber is more complicated than in the forced chamber. Mixing occurs when the flow enters though the lower opening and the effects of reflection from the far endwall produce horizontal variations in density as shown in figure 7. However, as discussed in § 2 we neglect these variations and treat the flow as being simply vertically stratified in the model. We assume that as new fluid enters, it lifts the existing fluid without any mixing. The results in figure 11 show that this assumption captures the main structure of the stratification. However, there are differences between the numerical calculations and the experimental observations and it is likely that these would only be reconciled by a more complex model including the effects of mixing and flow in the unforced chamber.

There is good qualitative and acceptable quantitative agreement between the model and the experiments for all aspect ratios, although as expected the agreement improves as R_A increases. The main qualitative difference is that the observed profiles are steeper than the calculated values, particularly near the bottom of the chamber. This difference may be a result of the gravity-driven currents that spread the fluid across the chamber over a finite depth rather than as an infinitely thin layer as assumed.

5. Conclusions

We have studied the flow between two coupled chambers driven by a single source of buoyancy in one of the chambers. The case we have considered is where the buoyancy source creates a plume and is located in the forced chamber, which is the same size or smaller than the unforced chamber. We have carried out laboratory experiments and developed a model for the flow.

In this section we take the orientation as that in § 2. Therefore the results in § 4 are taken upside down and the salt plume in the experiments is regarded as a heat plume here.

In the experiments, both chambers have displacement ventilation and the flow between them is in a transient state. The unforced chamber receives the hot buoyant fluid from the forced chamber and supplies the cold fresh ambient fluid to it.

The forced chamber has two distinguishable stages in the evolution of the density interface: the initial fast developing one, which is determined by the size of the forced chamber and the effective area of openings, and the later gradually evolving one, which responds to the changing stratification in the unforced chamber. The descending interface introduces hotter fluid into the buoyant layer in the forced chamber and the reduced gravity of this layer becomes larger with time.

The unforced chamber has a stable and transient stratification because the inflow fluid from the top opening is always lighter than the fluid that has previously entered. The exchange flow rate between two chambers depends on the pressure drops at the openings and the vertical pressure distribution varies with time in both chambers. The neutral level is not stationary like that in LLSS, but descends with time. The transient stratification in both chambers results in the pressure differences

at both openings changing, and this reduces the quantity of the exchange flow with time.

The mathematical model, based on evolution through quasi-steady states, is consistent with two extreme cases, one studied by Baines & Turner (1969) when $R_A = 0$ and one by LLSS (1990) when $R_A = \infty$. The model gives good agreement with the experiments in both chambers, especially when R_A is large.

The two-layer model in the forced chamber might not be very accurate at the small ratios, and the theoretical model overestimates the interface position when $R_A = 1$. Although the quantitative prediction is not fully satisfactory when R_A is small, qualitative observations confirm our transient model well. The unforced chamber has a more complicated flow than that simulated by the present numerical calculations. Nevertheless, the simple model used here has a good qualitative and acceptable quantitative comparison with experiments. Thus the observed mixing and gravity current dynamics are second-order effects. This is reasonable since the pressure is a result of an integral of the density distribution, and so differences in the details of the vertical profile are not so important.

This study completes the range of phenomena that occur in two connected interior spaces with a single heat source, where neither space is connected to the outside. It is restricted to times before warm fluid flows back into the forced chamber from the unforced chamber through the lower opening. After that occurs we expect an asymptotic state in which the fluid in the unforced chamber is heated uniformly at all heights. Since, in contrast to the filling box, the vertical velocity is constant with height there, we expect the asymptotic temperature gradient at heights between the two openings to be linear. As discussed in the introduction (see figure 3), cases with a single opening between two spaces lead to variations on the filling-box problem. When there are two (or more) openings the flow is topologically different, and the flow goes through a transient phase where there is displacement ventilation in both spaces. This cannot occur when there is only a single opening.

The results of this study show that when a smaller space with a heat source is connected to a larger unheated space, the evolution of the stratification occurs on two filling-box time scales. The initial adjustment takes place on the time scale of the smaller space, and is similar to the development in a space connected to an infinite environment. There is then a slower adjustment at later times that occurs on the time scale associated with the larger space. This means that the ventilation in a specific room depends not only on the geometry and openings in the room, but also on the size (and openings) of adjacent rooms. The details of this co-dependence are complex when there are multiple rooms connected together, but some simple rules are evident from the present study.

First, when all spaces within a building are enclosed, and do not communicate with the exterior, a heat source leads to a continuous increase of heat and the stratification is not steady. Second, in this case the time scale for the evolution depends on the size of the largest space. This means, for example, that in a shopping mall or office complex attached to an atrium the evolution of the stratification within individual shops and offices varies according to the size of the atrium. This means that if steps are taken to control the temperature within a shop, by locally changing conditions, it may never be possible to reach a desired set temperature.

Finally, it is clear from the discussion of the archetypal cases in figures 2 and 3 that the transient behaviour is strongly dependent on the geometry of the connecting openings between the spaces. Thus there should be careful consideration of the placement of openings when ventilation systems are designed.

The first author wishes to thank Ministry of Education in Taiwan providing the scholarship for part of this work. The research is also supported by a grant from California Energy Commission.

REFERENCES

Baines, W. D. 1983 A technique for the direct measurement of volume flux of a plume. *J. Fluid Mech.* **132**, 247–256.

Baines, W. D. & Turner, J. S. 1969 Turbulent buoyant convection from a source in a confined region. *J. Fluid Mech.* **37**, 51–80.

Cenedese, C. & Dalziel, S. B. 1998 Concentration and depth fields determined by the light transmitted through a dyed solution. In *Proc. 8th Intl Symp. on Flow Visualization* (ed. G. M. Carlomagno & I. Grant). ISBN 0953399109, paper 061 (CD rom).

Cooper, P. & Linden, P. F. 1996 Natural ventilation of an enclosure containing two buoyancy sources. *J. Fluid Mech.* **311**, 153–176.

Dalziel, S. B. 1993 Rayleigh-Taylor instability: experiments with image analysis. *Dyn. Atmos. Oceons* **20**, 127–153.

Hunt, G. R. & Kaye, N. G. 2001 Virtual origin correction for lazy turbulent plumes. *J. Fluid Mech.* **435**, 377–396.

Hunt, G. R. & Linden, P. F. 1999 The fluid mechanics of natural ventilation-displacement ventilation by buoyancy driven flows assisted by wind. *Building Environ.* **36**, 707–720.

Hunt, G. R. & Linden, P. F. 2001 Steady-state flows in an enclosure ventilated by buoyancy forces assisted by wind. *J. Fluid Mech.* **426**, 355–386.

Linden, P. F. 1999 The fluid mechanics of natural ventilation. *Annu. Rev. Fluid Mech.* **31**, 201–238.

Linden, P. F. & Cooper, P. 1996 Multiple sources of buoyancy in a naturally ventilated enclosure. *J. Fluid Mech.* **311**, 177–192.

Linden, P. F., Lane-Serff, G. F. & Smeed, D. A. 1990 Emptying filling boxes: the fluid mechanics of natural ventilation. *J. Fluid Mech.* **212**, 300–335 (referred to herein as LLSS).

Morton, B. R., Taylor, G. I. & Turner, J. S. 1956 Turbulent gravitational convection from maintained and instantaneous sources. *Proc. R. Soc. Lond.* A **234**, 1–23.

Turner, J. S. 1986 Turbulent entrainment: the development of the entrainment assumption. *J. Fluid Mech.* **173**, 431–472.

Wong, A. B. D. & Griffiths, R. W. 2001 Two-basin filling boxes. *J. Geophys. Res.* **106** (C11), 26929–26941.